Thesis for the degree of Master of Science

An *in vitro* evaluation of mesoporous titania implants

Hoda Mashadi Fathali

Supervised by Martin Andersson

Department of Chemical and Biological Engineering

CHALMERS UNIVERSITY OF TECHNOLOGY

Göteborg, Sweden, 2011

1. Abstract

The performance of an implant is highly related to its surface properties, such as surface roughness and chemistry. The aim of this study was to evaluate mesoporous cubic and hexagonal titanium dioxide coated implants. The implants ability to initiate apatite formation was assessed using an *in vitro* method, which is based upon simulated body fluids (SBF). Hexagonal and cubic mesoporous titania thin films were prepared via an evaporation induced self-assembly process and compared to non-porous titania. The surfaces were evaluated using three types of simulated body fluids (SBF); one containing dissolved salts that simulated the composition of human plasma, one with salts and Albumin, and one with salts and Alendronate (a well known osteoporosis drug). Characterization of the mesoporous titania was performed by transmission electron microscopy (TEM), scanning electron microscopy (SEM), contact angle measurement, small angle X-ray scattering (SAXS) and Nitrogen gas adsorption. The adsorption of ions, protein and Alendronate on the surfaces was monitored using quartz crystal microbalance with dissipation monitoring (QCM-D) and the apatite formation was studied as a function of time using SEM, TEM, X-ray diffraction (XRD), Fourier transform infrared spectroscopy (FTIR), and Raman spectroscopy. The results demonstrate that the mesoporosity on the titania surfaces initiated an enhanced calcium phosphate formation. The observation was seen using all three types of SBF's. Furthermore, the presence of Albumin and Alendronate in the simulated body fluid affected both the amount of formed calcium phosphate and its morphology.

Contents

2. Introduction

During the last decades, titanium has been the most frequently used biocompatible implant material [1].The bone integration, also known as osseointegration, of titania implants is related to their bone-bonding ability, which is due to the chemistry and topography of the implant surface. Many studies have been performed to improve the biocompatibility of implants by altering the surface topography using methods such as etching, sandblasting, electrochemical anodization and sol-gel chemistry with and without the presence of surfactants [2-6]. In this study, hexagonal and cubic mesostructured titania surfaces were prepared using sol-gel chemistry in the presence of surfactants (triblock copolymer, EO20PO70EO20, Pluronic P123). The surfactant was added in order to form mesoporous materials having a specific structure with well-defined pore sizes [6].

An essential requirement to achieve good bone-bonding ability of an artificial material is to ensure the formation of bone-like apatite on its surface when in contact with living tissue. [7, 8]. In order to investigate apatite formation on biomaterial surfaces, Kokubo et al developed an *in vitro* method using simulated body fluids (SBF). The method was invented about two decades ago to simulate *in vivo* conditions by using fluids having similar ions and ion concentration as in the human blood plasma. Using this method, the bioactivity of implant materials can be predicted in an *in vitro* system. Since the discovery, Kokubo and his coworkers have further developed the technique using new SBF recipes, with the possibility of using the SBF solution for longer times without getting precipitations[9].

The presence of proteins is believed to play an important role in biomineralization processes as well as affecting the activation of implants. The proteins also play a fundamental role in the cell behavior in regards to their interaction with biomaterials. Albumin constitutes about half of the proteins in human blood plasma (Figure 1a) and investigations have been done using bovine serum Albumin (BSA) containing SBF´s. These studies were performed to evaluate the effect of Albumin on the nucleation rate, crystallinity and morphology of formed apatite [10-12]. In this present project, the effect of Albumin was evaluated on hexagonal and cubic mesoporous titania surfaces and a comparison was assessed with non-porous titania surfaces.

Alendronate is a bisphosphonate drug, which is extensively used to treat several bone diseases, like osteoporosis (Figure 1b). Previous studies have shown that bisphosphonate has the ability to inhibit the bone resorption by binding tightly to apatite and decrease the function

of osteoclasts [13-16]. In the present study, the apatite formation onto mesoporous and non-porous titania with the presence of Alendronate on the implant surface was investigated. Also the effect of Alendronate when dissolved in SBF was studied in relation to the nucleation, crystallinity and morphology of the formed apatite.
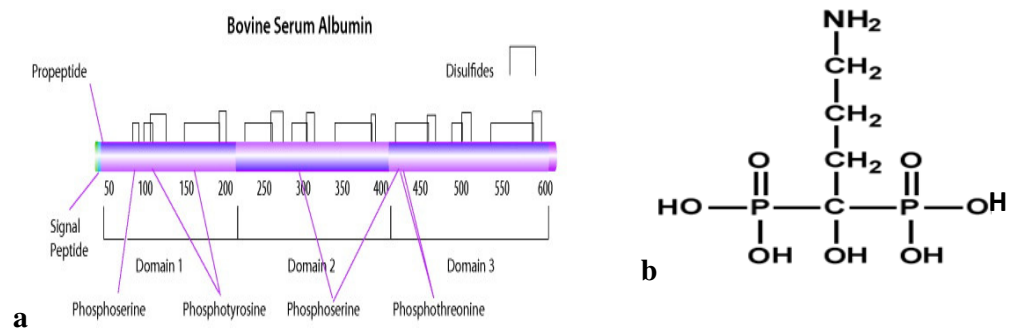
Figure 1: a) Albumin [17] and b) Alendronate structures

3. Material and methods

3.1. Surface preparation

In order to synthesize mesoporous cubic and hexagonal as well as non-porous titania thin films, an evaporation self-assembly procedure was employed. To hydrolyze titanium alkoxide, 4.2 g of titanium (IV) tetraethoxide (TEOT, 95% Aldrich) was added drop-wise at room temperature under vigorous stirring in 3.2 g concentrated hydrochloric acid (12.1 M). The highly acidic condition was required to prevent immediate sedimentation of TiO_2. To form cubic and hexagonal mesostructured titania films, specific amounts of surfactant were essential and triblock copolymer (EO20PO70EO20, Pluronic P123, Aldrich) was used. The precise amount of P123, as listed in Table 1, was dissolved in ethanol (200 proof) and the titania and surfactant solutions were mixed together and stirred [6]. The Final solutions were stirred at room temperature for 15 min followed by spin coating on the surface of commercially pure titanium circular discs (grade 3) with 8 mm diameter and 3 mm thickness. The spin speeds were optimized to avoid crack formation, see Table 1. After the spin-coating the films were aged overnight at room temperature and then calcined by heating to 400°C at the rate of 1°C/min to remove surfactant and increase cross-linking of titania .

Table 1: The amounts of P123 (g), Ethanol (g) and the speed of spin-coating (r.p.m)

Structure	P123 (g)	Ethanol (g)	Spin-coating speed (r.p.m)
Non-porous	0	17	8000
Hexagonal mesoporous	2.3	17	10000
Cubic mesoporous	1.0	17	6000

3.2. SBF immersion

Modified SBF (m-SBF) as described by T. kokubo and coworkers [9] was applied in the present study. It was prepared by dissolved reagents, which is listed in Table 2 at 37°C under stirring and adjusted to a final PH of 4.7 using HCl. Modified SBF was chosen since it has the most similar ion concentrations as in the human plasma and for that is has less carbonate (HCO_3^-) in order to avoid sedimentation, see Table 3. Three types of SBF´s were prepared, one pure m-SBF, one m-SBF with Albumin and one m-SBF with Alendronate.

36 titanium discs were coated with thin films having cubic and hexagonal mesostructures as well as non-porous titania (n=12 for each group). The discs were immersed in 25 mL m-SBF in separated sealed polystyrene vials and kept at 37°C. Once a week the m-SBF solutions were changed to freshly prepared solutions. After 1, 2, 4 and 8 weeks, 3 titanium discs from each group were lifted out of the solution and rinsed with milli-q water to remove precipitated material, which was loosely attached on the surface and then they were left to dry at room temperature.

To evaluate the effect of Albumin in SBF, 4.5 mg/ml Albumin (from bovine serum, Sigma Aldrich) was added [10]. 36 specimens were prepared with the same procedure as described above and they were immersed in m-SBF/Albumin. Evaluation was performed after 1, 2, 4 and 8 weeks.

Two evaluation procedures were chosen to evaluate the effect of Alendronate. In the first procedure, 36 specimens were soaked primarily in Alendronate dissolved in milli-q water (0.2 mg/ml) for 30 minutes to have a saturated layer of Alendronate on the surface, dried in air at room temperature and then immersed in SBF. In the second procedure, 0.1 mg/ml Alendronate was added to SBF solution [18, 19] and its effect was studied after 1, 2, 4 and 8 weeks.

Table 2: Reagents, their purities and amounts for preparing 1000 mL of m-SBF

Reagents	Purity	m-SBF
NaCl	> 99.5	5.403 g
NaHCO$_3$	> 99.5	0.504 g
Na2CO3	> 99.5	0.426 g
KCl	> 99.5	0.225 g
K2HPO4.3H2O	> 99.0	0.230 g
MgCl2.6H2O	> 98.5	0.311 g
0,2 M NaOH	-	100 mL*
HEPES	> 99.9	17.892 g*
CaCl2	> 95.0	0.239 g
Na2SO4	> 99.0	0.072 g

*HEPES was dissolved in 100 mL of 0.2 M NaOH aqueous solution before addition to SBF.

Table 3: Ion concentration in human blood plasma and modified-SBF

(mM)	Na$^+$	K$^+$	Mg^{2+}	Ca^{2+}	Cl$^-$	HCO$_3^-$	HPO$_4^{2-}$	SO$_4^{2-}$
Human blood plasma	142.0	5.0	1.5	2.5	103.0	27.0	1.0	0.5
modified-SBF	142.5	5.0	1.5	2.5	103.0	10.0	1.0	0.5

3.3.Evaluation of surfaces

3.3.1. Contact angle measurement

Contact angle measurements were performed using a dynamic adsorption tester (DAT 1100, FIBRO systems AB, Sweden). This technique is used to provide information about the interfacial free energy of a surface. It is performed by measuring the equilibrium contact angle (θ) of a liquid drop on a solid surface and the surface free energy is calculated using Young's equation.

Equation 1 $\qquad \gamma_{SV} = \gamma_{SL} + \gamma_{LV} \cos(\theta)$

γ_{SV}, γ_{SL} γ_{LV} are the interfacial tension between the solid-vapor, solid-liquid and liquid-vapor [20]. The most convenient method to determine the value of the interfacial free energy of a surface is to draw a Zisman plot [21]. This was performed by measuring the contact angle (θ) of different liquids with known surface tension (γ_{LV}), as listed in Table 4. This was performed on the hexagonal, cubic and non-porous titania surfaces. The cos (θ) was measured for the different liquids and were plotted against γ_{LV} and the surfaces energy were defined as cos (θ) =1.

Table 4: Surface tension of the different liquids that was used for the contact angle measurements

Liquid	γ_{LV} (dyns/cm)
Penthanol	25.7
Octanol	28.0
Oleyl alchohol	31.7
Propanol	29.6
Water	73

3.3.2. Nitrogen adsorption

The nitrogen adsorption experiments were performed on samples that were degassed in a vacuum oven at 120° C for 3 hours. The measurements were done using a Micrometrics Tristar (Norcross, GA). The aim of the measurements were to obtain information about surface area and pore size distribution of the mesoporous surfaces and compare these to the non-porous surface and to make a comparison with the pore sizes obtained by TEM. The experiments were done by degassing the samples under control pressure and temperature with nitrogen gas. By increasing the pressure, the amount of gas molecules that adsorbs will increase. By measuring the equilibrium pressure and by applying the gas laws, the amount of adsorbed gas molecules on the sample is calculated, which can be used to determine the surface area and pore size in the sample. [22, 23]

3.3.3. QCM-D

Quartz crystal microbalance with dissipation monitoring (QCM-D) was used to investigate the adsorption of ions and apatite formation on the titania surfaces. A Q-sense E4 with 14 mm titania QCM-D crystals was used (Q-sense AB, Gothenburg, Sweden). The crystals were coated with hexagonal, cubic and non-porous titania by spin coating using the same procedure and speeds as described above for the titanium discs (Table 1).

QCM-D is an analytical technique, which measures adsorption of molecules on an oscillating quartz crystal. The adsorbed mass is calculated by monitoring the resonance frequency (Δf) of piezoelectric quartz crystal. Moreover, elastic and viscoelasticity behavior of the adsorbent is monitored by dissipation. For rigid layers, which have low dissipation, the Saurbrey equation is used to determine the mass adsorbed from the measured frequency shift (Equation 2).

Equation 2 $\Delta m = -C * \Delta f$

, where C is the mass sensitive constant, $C = 17.7$ $ng.cm^{-2}.Hz^{-1}$ and Δf is the measured frequency shift which is $\Delta f_n / n$, where n is the overtone (overtone number 7 was chosen) [24, 25].

The coated QCM-D crystals were rinsed with Helmanex (2%) for 15 min, milli-q water for 5 min, dried by nitrogen gas followed by an UV-ozone treatment for 15 min. The adsorption of three types of SBF´s on hexagonal, cubic and non-porous surfaces was monitored during 40 h and the results were interpreted using Q-tools software (Q-sense AB, Gothenburg, Sweden).

3.3.4.   SEM

Scanning electron microscopy (SEM) is a technique where an electron beam is used as source instead of photons to acquire high resolved images of a material. The electron beam is accelerated by applying a potential (5 kV was chosen in this study), focused and scanned across the surface. With the SEM, information about morphology, shape and size of nano-sized features can be obtained. The SEM used was a Leo Ultra 55 FEG SEM (Leo Electron Microscopy, Cambridge, UK)

3.3.5.   TEM

In Transmission Electron microscopy (TEM) accelerated electrons at high voltages are used (up to 400 kV) and the interaction between the electrons and the sample gives information about structures with a very high resolution (a few angstrom). The TEM used was a JEOL-1200 EX II TEM operated at 120 kV (Jeol, Tokyo, Japan). Sample preparation for TEM analysis was done by scraping of the titania coating and formed apatite and disperse it in ethanol (proof 200) followed by sonication for 2 min. A drop of the dispersion was left to dry on TEM grids (Lacey Formvar/carbon 300 mesh, caspilor, Sweden) before inserted into the microscope.

3.3.6.   XRD

X-ray diffraction (XRD) is a method where X-ray beams are interacting with the sample. At a certain angle the incident beam will interfere with the atomic placement in the crystal structure of the sample and will diffract a certain intensity beam, which is detected. The detected signal contains information about the crystal structure of a crystalline material according to Bragg's law (Equation 3).

Equation 3   2d sinθ= nλ

, where n is any integer, d is the lattice spacing, θ is the angle and λ is wavelength of the incident beam. Moreover, the crystal structure was identified using JCPDS (Joint Committee on Powder Diffraction Standards).

3.3.7.   SAXS

Synchrotron radiation SAXS was performed at MAX-Lab beam station line I911 (Lund, Sweden). It is an analysis method to determine the intermolecular structure by X-ray scattering at low angles (< 10°). With this technique it is possible to determine if the mesoporous sample is lamellar, hexagonal or cubic. It also provides information about the pore size in the length scale of 1-100 nm and pore distributions.

3.3.8.   FTIR

Fourier transform infrared (FTIR) is a technique where infrared radiation passes through the sample (if run in transmission mode). Some of the IR radiation will be absorbed by the sample and some will be transmitted. FTIR can be used to identify the sample components and also to determine the quantity of the components in the sample. In the present study FTIR was performed to characterize the formed apatite on the titania surfaces. Sample preparation was done by grinding the formed apatite, obtained after four weeks, with KBr to prepare tablets. The FTIR used was a PERKIN ELMER 2000 FT-IR.

3.3.9.   Raman spectroscopy

In Raman spectroscopy, photons of a laser light are used as the source of energy and the technique is based on the inelastic scattering of monochromatic light. The photons of the laser light will be absorbed by the sample and then reemitted. The reemitted photons provide information due to the vibrational, rotational and low frequency transmission in the molecular structures of the sample.

Raman spectra were collected at room temperature by a liquid-nitrogen cooled CCD detector connected to a Dilor XY spectrometer. The single grating had a groove density of 1800

grooves/cm and the diffracted light was dispersed over a distance of 30 cm before reaching the detector. A micro configuration with a 100x objective was employed and the 514.5 nm line from an Ar+ laser was used as excitation source. The laser power was kept at ~6 mW at the sample with a spot size of 1 μm. Raman spectroscopy was done by Johan Bielecki a material physics department, Chalmers.

4. Results and Discussion

4.1. Characterizations of mesoporous titania surfaces

Cubic and hexagonal mesoporous titania thin films were successfully formed on the titanium discs [6]. SEM images of hexagonal, cubic and non-porous surfaces indicated hexagonal structures with a cylindrical pattern and the cubic structure with connecting rod line outline motifs (Figure 2). Figure 3 illustrates a schematic for hexagonal, cubic and non-porous titania surfaces formed in the presence of P123 surfactant.
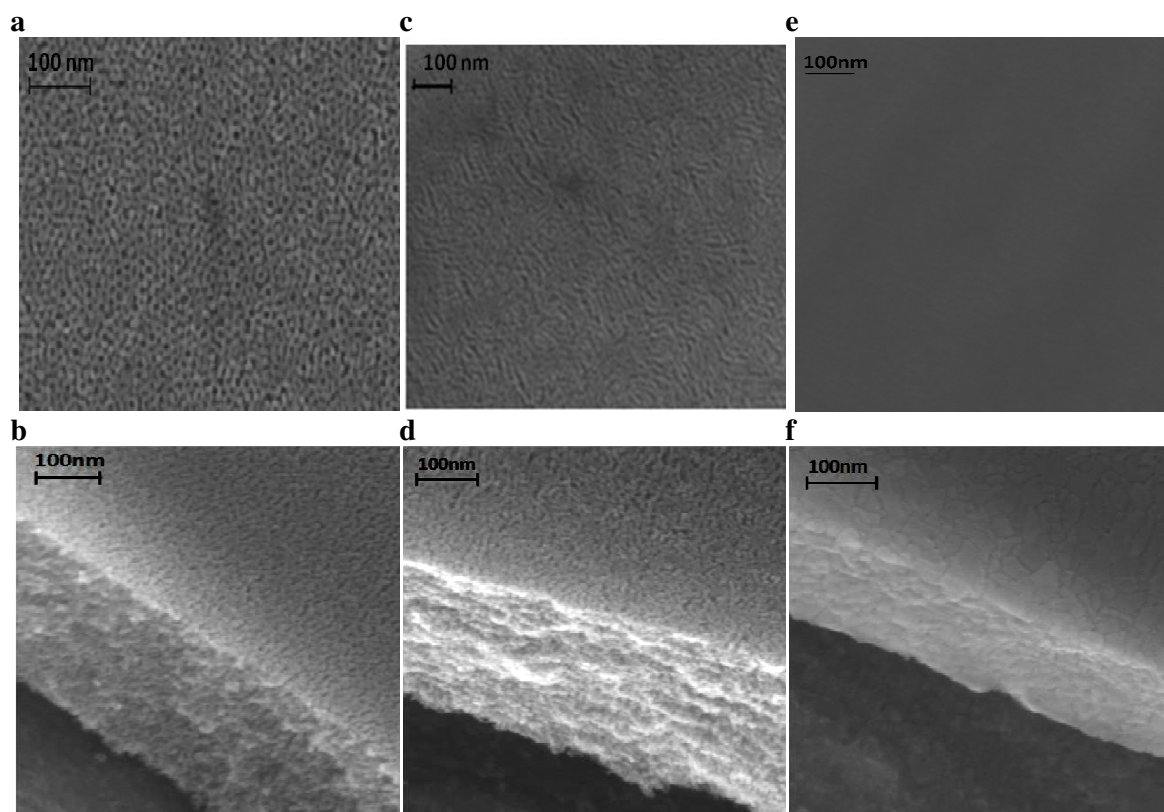
Figure 2: SEM images of a, b) cubic, c, d) hexagonal, e , f) non-porous titania surfaces.
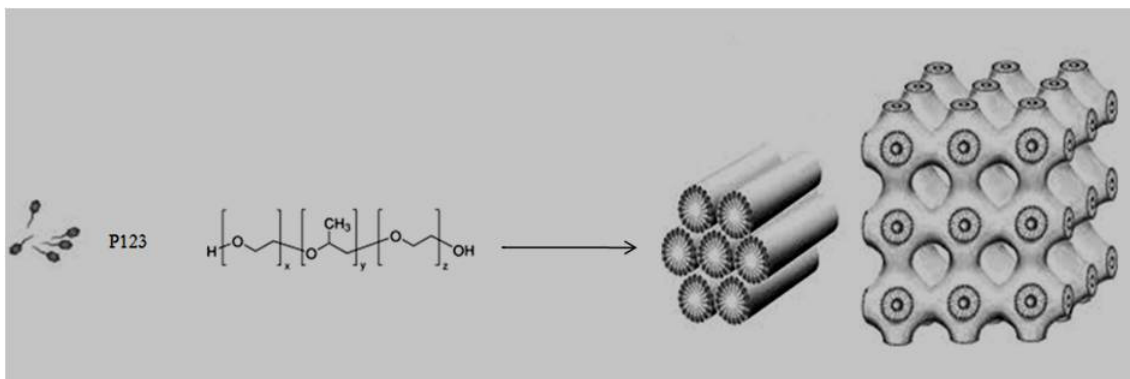
Figure 3: Schematic for hexagonal and cubic formed structures using P123 surfactant

According to the SEM micrographs (Figure 2 b, d, f), the thickness of the coating layers on the titanium discs were about 250 nm for cubic and hexagonal mesostructures and 150 nm for non-porous titania. To obtain information about the surface area, pore size and periodicity of the pores, TEM, Nitrogen gas adsorption and SAXS measurements were done. By contact angle measurements the hydrophilicity of the mesoporous and non-porous titania surfaces were obtained.

The hexagonal structure, which consisted of long cylinders arranged in a hexagonal pattern, had a high specific surface area as obtained from the nitrogen gas adsorption measurements (Table 5). The cubic phase was built up of discrete cubic patterns, which formed by connecting rod-like outlines and the openings of the pores were accessible on the surface.

In Figure 4, a TEM micrograph illustrating the pores present on the cubic and hexagonal surfaces are seen. The pores size was estimated to about 6 nm for both the hexagonal and cubic structures. In contrast, Nitrogen gas adsorption results instead gave 4 nm pore size for the same materials (Table 4). The difference between the values are probably due to the fact that nitrogen adsorption also measures the existing micropores in the materials, hence the pore sizes obtained by Nitrogen adsorption will appear smaller [26].
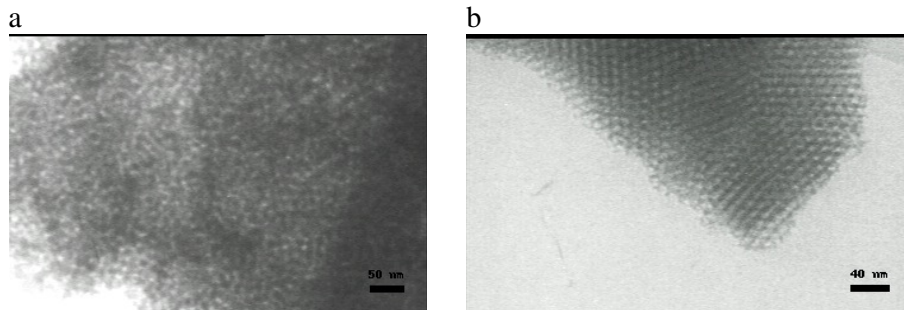
Figure 4, TEM images of a) cubic and b) hexagonal titania mesoporous surfaces

Table 5: Specific surface areas and pore sizes obtained from nitrogen gas adsorption and TEM measurements

Titania surfaces	Hexagonal	cubic	Non-porous
Specific surface area (m^2/g)	127	63	52
Pore size (nm) By N_2 adsorption	4	4	-
Pore size (nm) By TEM	6	6	-

SAXS measurements were performed on prepared hexagonal and cubic mesoporous titania (Figure 5). The hexagonal structure is supposed to have the peak position ratio 1: $3^{1/2}$: 2 related to the diffracted peaks (100), (110) and (200) [6]. The direct observation indicated only the (100) and (200) peaks, which might be due to the orientation of the unit cells. In the cubic phase, one peak was observed which indicated presence of a mesoporous structure but it wasn't possible to do a clear identification of the exact phase. According to the position of the Bragg's peaks, it is most probably a worm-like cubic structure. The broad width of the peaks in cubic and hexagonal titania phases also indicate distorted structures. [6, 27, 28]
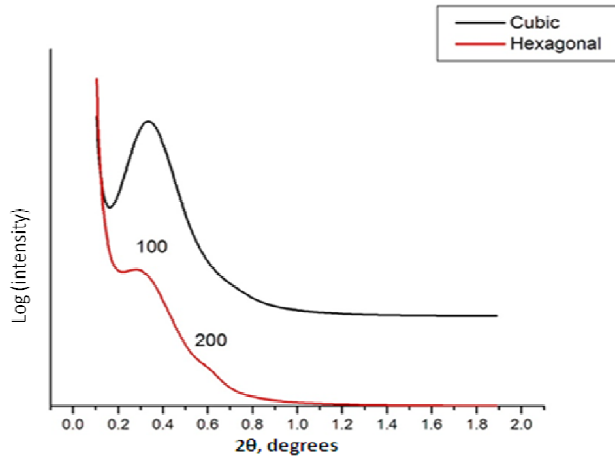
Figure 5 Synchrotron radiation SAXS on cubic and hexagonal titania performed at MAX-Lab, Lund

The hydrophilicity and free surface energy of the surfaces were determined by contact angle measurement using the Young's equation together with Zisman plots [20, 21]. The results indicated higher surface energy on mesoporous titania surfaces in comparison to the non-porous surface (Figure 6). On the cubic surface a relatively high surface energy was obtained 14.4 dyn/cm. For the hexagonal surface, the surface energy was lower, 12.1 dyn/cm. A higher surface energy indicates a more hydrophilic surface.
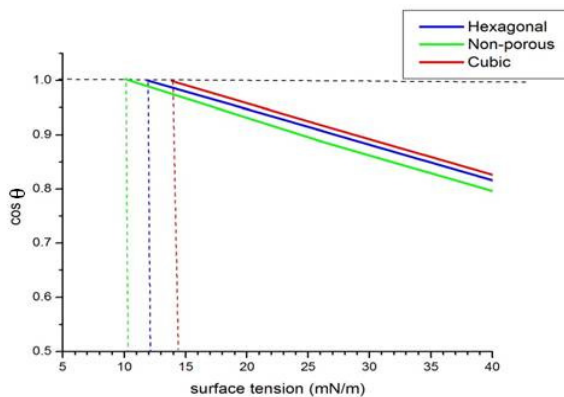
Titania surface	Non-porous	Hexagonal	cubic
Free surface energy, γ_{ls} (mN/m)	10.2	12.1	14.4

Figure 6: Zisman plots obtained from contact angle measurements on the hexagonal, cubic and non-porous titania surfaces. In the table, the free surface energies from the Zisman plots are presented.

4.2. SBF adsorption on mesoporous and non-porous titania thin films

In order to do study the initial adsorption of ions from the three types of SBF's on hexagonal, cubic and non-porous titania surfaces, QCM-D measurements were performed. QCM-D results illustrated adsorption of ions in the presence of SBF. Also, Albumin and Alendronate adsorption on the surfaces were studied and a comparison was done on the adsorption of ions in the presence of Albumin and Alendronate.

Figure 7 shows QCM-D results from experiments with SBF, SBF/Albumin and SBF/Alendronate on titania surfaces. The typical exponential frequency declines that are seen in the QCM-D plots represent a macromolecular adsorption. From the graphs a general trend can be observed in that the frequency shift was much greater on the mesoporous surfaces in comparison to the non-porous titania surface. The increase in mass for the first five hours in the presence of SBF (Figure 7a) is originating from ion adsorption. Since the titania surface is slightly nagative at neutral pH, the first layer of ion adsorption is probably positively calcium ions, which then is subsequently followed by negatively phosphate ions leading to the formation of calcium apatite [24]. Figure 9 illustrates a schematic based from the QCM-D results illustrating the ion adsorption on titania surface and subsequent apatite formation.

a

b

c

d

e

f
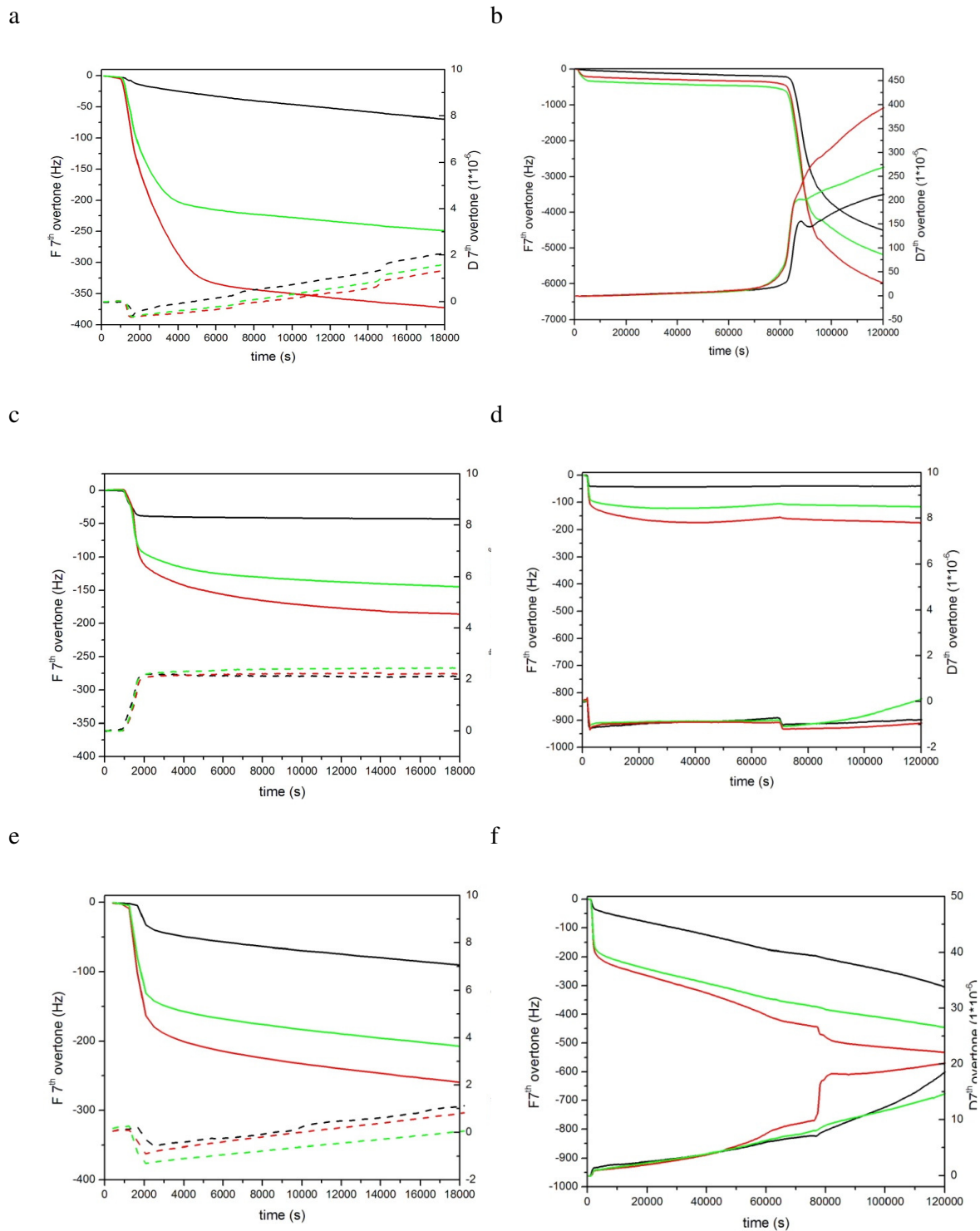
Figure 7: QCM-D results for a) SBF b) SBF/Albumin, c) SBF/Alendronate after 5 hours and d) SBF e) SBF/Albumin, f) SBF/Alendronate after 33 hours. Black line is on nonporous, green line on cubic and red line on hexagonal mesoporous titania coated crystals.

a   b
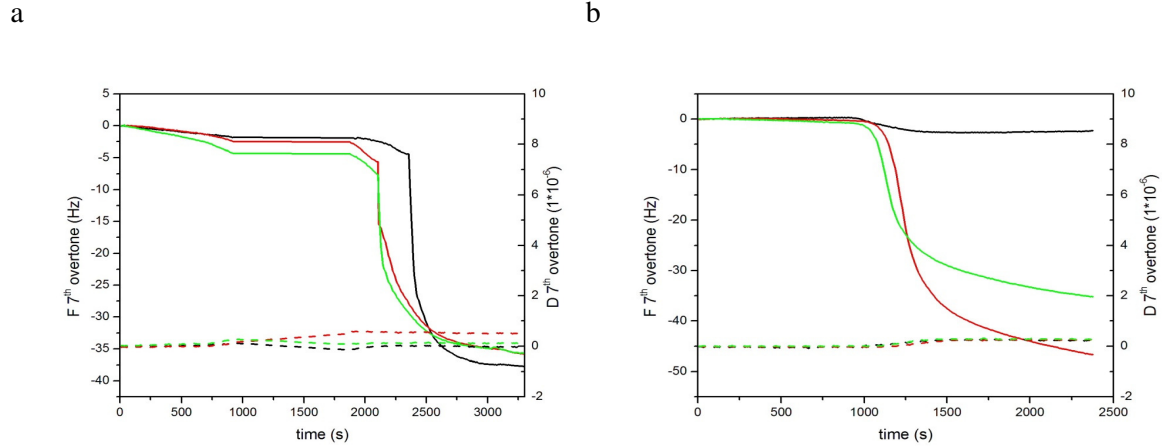
Figure 8: QCM-D results showing a) Albumin, b) Alendronate adsorption. Black line is on non-porous, green line on cubic and red line on hexagonal mesoporous titania coated crystals.
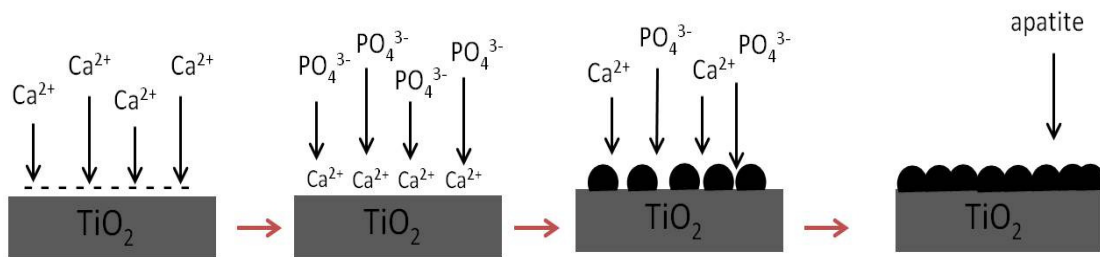
Figure 9: Schematic of ion adsorption on titania surface and apatite formation

Figure 8a shows Albumin adsorption on titania coated surfaces. Regardless of porosity, Δf and ΔD were similar on mesoporous and non-porous surfaces. The size of Albumin is roughly 4*4*14 nm (sigma Aldrich), which is bigger than the size of the pores on the mesoporous surfaces, and therefore the porosity of surfaces does not significantly influence the Albumin adsorption. Moreover, the dissipation results illustrated a low shift, which indicated the Albumin is adsorbed on the surfaces as a rigid layer.

The presence of Albumin in the SBF solution caused adsorption of Albumin onto the surfaces, which is in competition with the ion adsorption. This was observed as a significant decrease in ion adsorption in the first hour when compared to pure SBF. Figure 7c shows SBF/Albumin adsorption. More adsorption was observed on the mesoporous surfaces compared to on the non-porous surface, which was due to ion adsorption inside the pores.

20

The presence of proteins during the apatite formation effects both the nucleation step and the crystal growth process [12]. The presence of Albumin influenced the calcium phosphate nucleation on all surfaces and caused inhibition. Moreover, the apatite crystal structure was affected and the crystallization was hindered [12, 29]. Existence of Albumin in SBF simulated a solution which is closer to human plasma. Due to the presence of carbonate in the fluid, a variation in the apatite structure can occur due to substitution of CO_3^- with OH^- or PO_4^- [30]. Adsorption of Albumin to the surfaces acted as a linkage between Ca^+ and PO_4^- ions and favored the formation of carbonated apatite [31]. Moreover, the decline in adsorption of ions and mineralization were observed after longer times compared to pure SBF (Figure 7d)

Alendronate molecules adsorbed on the surfaces during the first hour (Figure 8b) and its mass was higher on the hexagonal surface then on the cubic one, which both were much higher than on the non-porous surface. Presence of Alendronate in the SBF caused a co-precipitation of ions and Alendronate. Alendronate has a P-C-P backbone, which is resistant to hydrolysis and causes reduction of ions. The Alendronate adsorption on the surfaces has two targets; the $NH_2^{+.}$ site, which is responsible for bone resorption and the OH^- site that has a high affinity for binding to calcium ions and cause hindering of hydroxyapatite formation [16]. Therefore, Alendronate causes less active sites to be available on the surface for calcium ion binding. QCM-D results from SBF/Alendronate adsorption showed lower mass adsorption of ions in contrast to SBF results on all surfaces. Moreover, also in these situations higher adsorption was observed on the hexagonal surface (Figure 7e and f).

In the first hours of observation, the dissipation was observed to be low for all the investigated combinations, which indicates that the adsorbed material was rigid. At longer times, the dissipation was increased in combination with a higher decline in frequency. Hence, for the first hours it is possible to calculate the mass adsorption using the Sauerbrey equation (Equation 2), which indicated higher mass adsorption on hexagonal and cubic mesoporous surfaces in comparison to non-porous titania. A significant decline in adsorbed mass was observed in the presence of Albumin and Alendronate Figure 10).

	SBF	SBF/Albumin*	SBF/Alendronate*
Non-porous	1255	128	1302
Cubic	4403	1425	3572
Hexagonal	6606	2189	3823
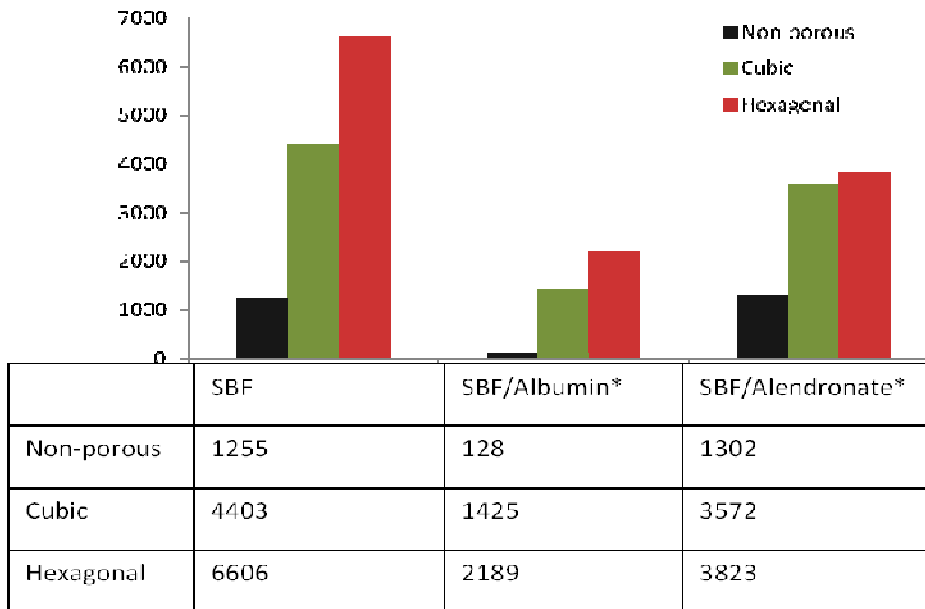
Figure 10: Areal mass adsorption (ng/cm^2) calculated by Sauerbrey equation on the hexagonal, cubic and non-porous surfaces in the presence of SBF, SBF/Albumin and SBF/Alendronate after five hours

* The mass adsorption in the presence of SBF/Albumin and SBF/Alendronate is presented without the mass adsorption of Albumin and Alendronate, which is listed in Table 6.

Table 6: Mass adsorption of Albumin and Alendronate using the Sauerbrey equation

	Albumin	Alendronate
Non-porous	632	41
Cubic	600	616
Hexagonal	594	818

4.3. Characterizations of adsorbed layers on mesoporous and non-porous titania thin films

SEM micrographs after one week indicated different adsorption behavior on hexagonal, cubic and non-porous surfaces.   It was obvious that the presence of mesostructures provided higher apatite formation. Figure 11 shows apatite formation on the cracks of surfaces. Higher apatite formation on the crack walls was significant on the hexagonal titania. On the cubic surfaces less apatite was attached to the crack's wall and on non-porous surfaces, no apatite formation was observed on the cracks. This adsorption behavior was similar in the presence of Albumin and Alendronate.

SEM results after 1, 2, 4 and 8 weeks of immersion in SBF, SBF/Albumin and SBF/Alendronate indicated calcium phosphate formation on all hexagonal, cubic and non-porous surfaces. The calcium phosphate formation increased with time and all surfaces were totally covered after 4 weeks of immersion. Therefore no significant differences were obtained on the different surfaces after longer times. However, the calcium phosphate crystals, which were formed in the presence of the three types of SBFs were different. Figure 12 shows SEM images of calcium phosphate crystals in the presence of SBF, SBF/ Albumin and SBF/Alendronate.

Figure 12 c and d indicate apatite formation after two and four weeks in the presence of SBF/Albumin. The influence of Albumin on the morphology of the crystals was high, as seen in the SEM micrographs. The darker parts on the surface in Figure 12 c were due to the presence of protein.

Two types of SBF/Alendronate sample preparation were prepared. In the first type, the titanium coated discs were soaked in Alendronate (0.2 mg/ml Alendronate) for 15 min, dried in air at room temperature and then soaked in SBF. In the second type, 0.1 mg/ml Alendronate was added to the SBF solution and discs were soaked in SBF/Alendronate for 1, 2, 4 and 8 weeks. The SEM micrographs indicated the same results for the two types in the first week as can be seen in Figure 12 e. After 2 weeks the effect of Alendronate was not observed for the type where the discs were soaked in Alendronate prior to being immersed in SBF. This is most probably due to the low concentration of Alendronate and that it is "used" up already after two weeks. But in the second type of SBF/Alendronate preparation the effect of Alendronate on crystals growth were see also after longer times (Figure 12 f). In

SBF/Alendronate, the size of the calcium phosphate crystals was reduced in comparison with samples in SBF.
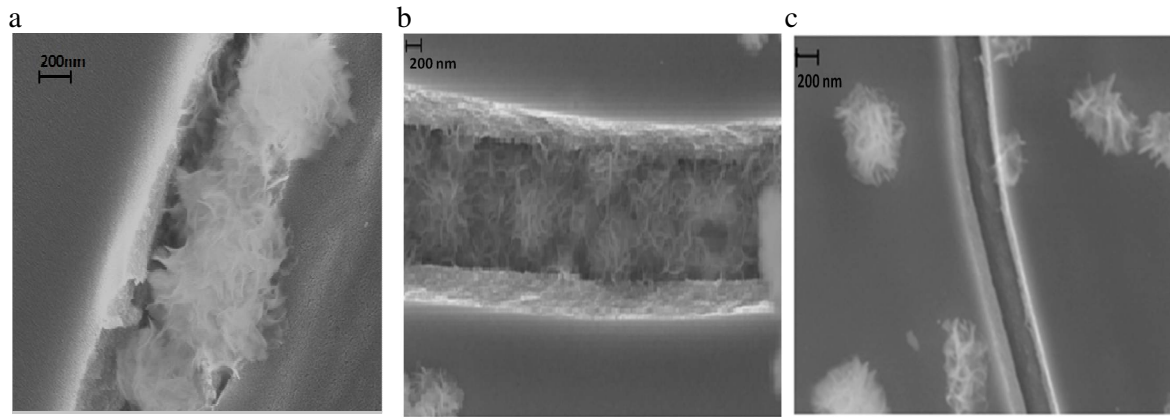
Figure 11: SEM images of apatite formation on a) hexagonal, b) cubic, c) non-porous titania surface
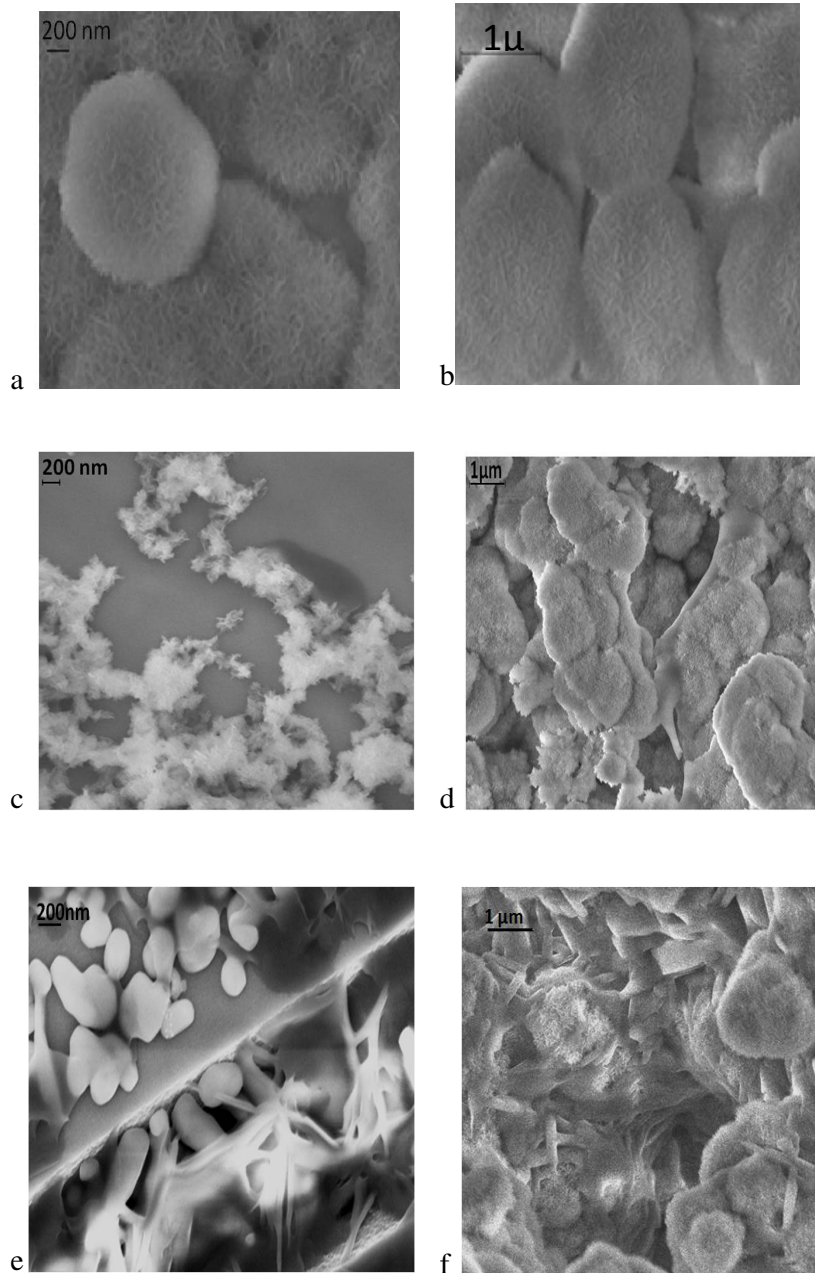
Figure 12: SEM images of apatite formation after two weeks on hexagonal surfaces in a) SBF, b) SBF/Albumin, c) SBF/ Alendronate and after four weeks in d) SBF, e) SBF/Albumin, f) SBF/Alendronate.

TEM micrographs of crystals formed in SBF, SBF/Albumin and SBF/Alendronate were different (Figure 13). The size of the formed apatite in SBF was (7±2 nm) * (50±8 nm) and in SBF/Albumin they were (2±1nm)* (25±5 nm), which indicated hindrance in crystal growth in the presence of Albumin. This result correlates well with the SEM micrographs. In the

presence of SBF/Alendronate an amorphous structure was observed, which was due to high concentration of Alendronate in SBF (second type) leading to hindering of the crystal formation.
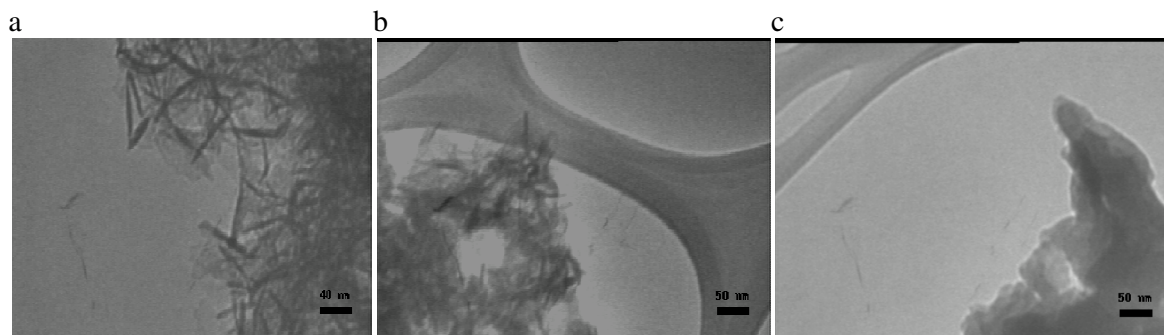
Figure 13: TEM images of hydroxyapatite formation in a) SBF, b) SBF/Albumin, c) SBF/Alendronate.

Figure 14 a shows XRD results, which were obtained after 4 weeks of immersion in SBF, SBF/Albumin and SBF/Alendronate. Hydroxyapatite formation was observed on the surfaces in the presence of SBF and SBF/Albumin. But on the surfaces of the discs in the presence of SBF/Alendronate, sodium magnesium chloride formation was detected instead, which was due to high concentration of Alendronate in the solution. This caused hindering in the apatite formation and the same results were obtained from the TEM investigation.

Figure 14 b presents the results of the FTIR after one week of immersion in SBF, SBF/Albumin and SBF/Alendronate. The results indicated presence of calcium phosphate in SBF and SBF/Albumin, which correlated well with the XRD results. FTIR result from the sample in the presence of SBF indicated a double peak at 560, 601 cm^{-1} being a P-O-P bending mode and 1027 cm^{-1} which was originating from P-O stretching PO_4^{3-} [32, 33]. The absorption peaks at 872 cm^{-1} and 1459 cm^{-1} were assigned as a carbonate bond from the apatite structure [34, 35]. A broad peak at 3421 cm^{-1} and 1611 cm^{-1} are due to stretching bonds from OH^- groups in the hydroxyapatite structure [33, 35, 36]. Additionally, the results indicate the presence of H_2O, which was revealed as being decreased after heating.

Calcium phosphate obtained by immersion in SBF/Albumin (Figure 14b) predicted the presence of proteins on the surface. C=O stretching band at 1600–1700 cm^{-1} was due to the amide I, at 1500–1550 cm^{-1}, N–H deformation for the amide II was significant. N–H deformation at 1200–1300 cm^{-1} originated from the amide III band [37-39]. The amide III peak was correlated with the carbonate peak at 1459 cm^{-1}.

FTIR results from SBF/Alendronate presented a decline in the phosphate peak, which could be due to hindered hydroxyapatite formation. Moreover, some unidentified peaks about 1200 cm^{-1} were detected due to presence of new components.

Raman spectroscopy was performed by Johan Bielecki at material physics, Chalmers on the coated mesoporous and non-porous titania discs after being soaked for four weeks in SBF, SBF/Albumin and SBF/Alendronate, The Raman results are presented in Figure 15. In the spectra there was a strong C-H peak together with unidentified peaks in the 800-1500 cm^{-1} region. These peaks weren't as strong in the samples containing Albumin in the SBF. The peak corresponding to phosphate ν_1 vibrations are completely missing but other phosphate peaks were present. One tentative explanation is that the crystal structure of this sample is changed in some way, which caused "missing" peaks the in Raman spectra. In all three types of samples no OH signals can be found and it could be related to the width of the phosphate ν_1 in 18-20 cm^{-1} and from this aspect the samples are very bone-like. [40]

a

b

28
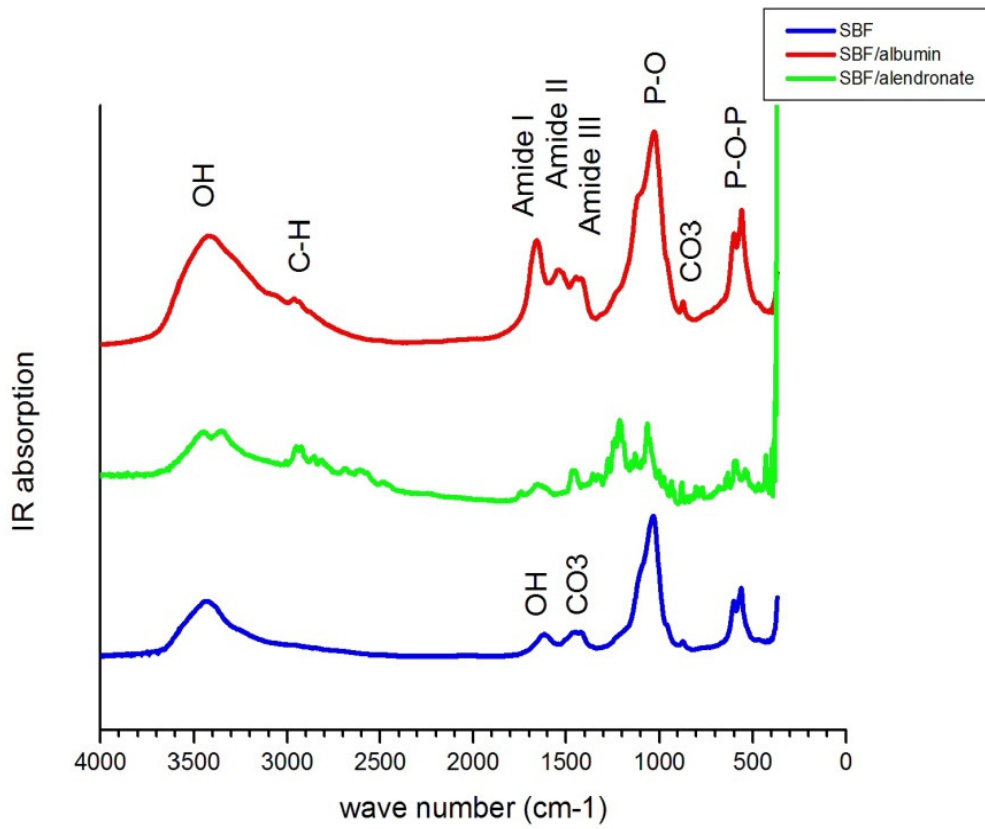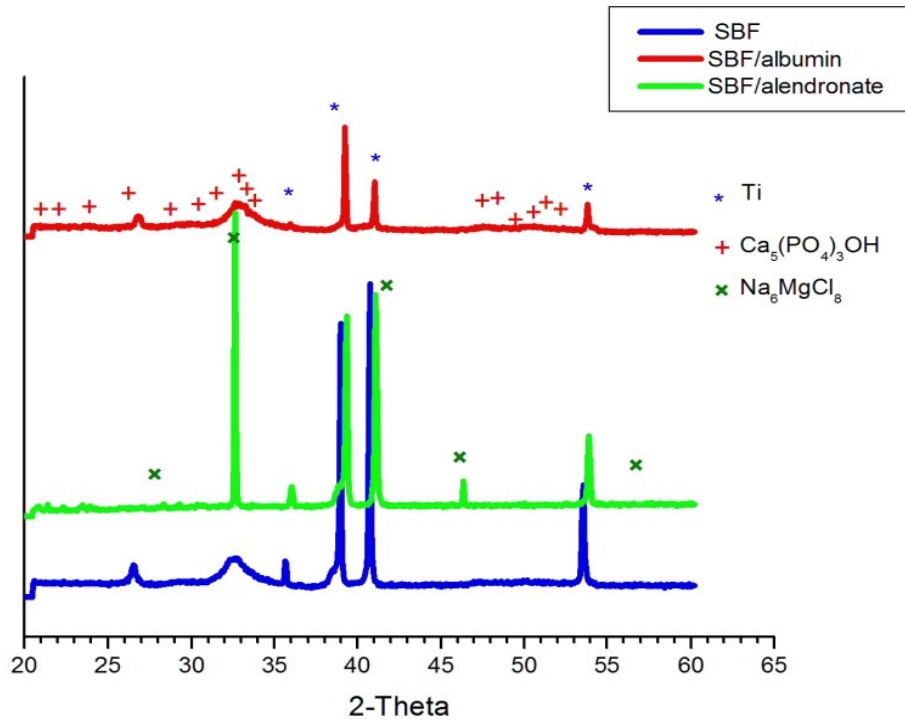
Figure 14: a) XRD and b) FTIR on titania surfaces after 4 weeks immersion in SBFs. Blue line is sample from SBF immersion, red line from SBF/Albumin and green line from SBF/Alendronate.

a

b
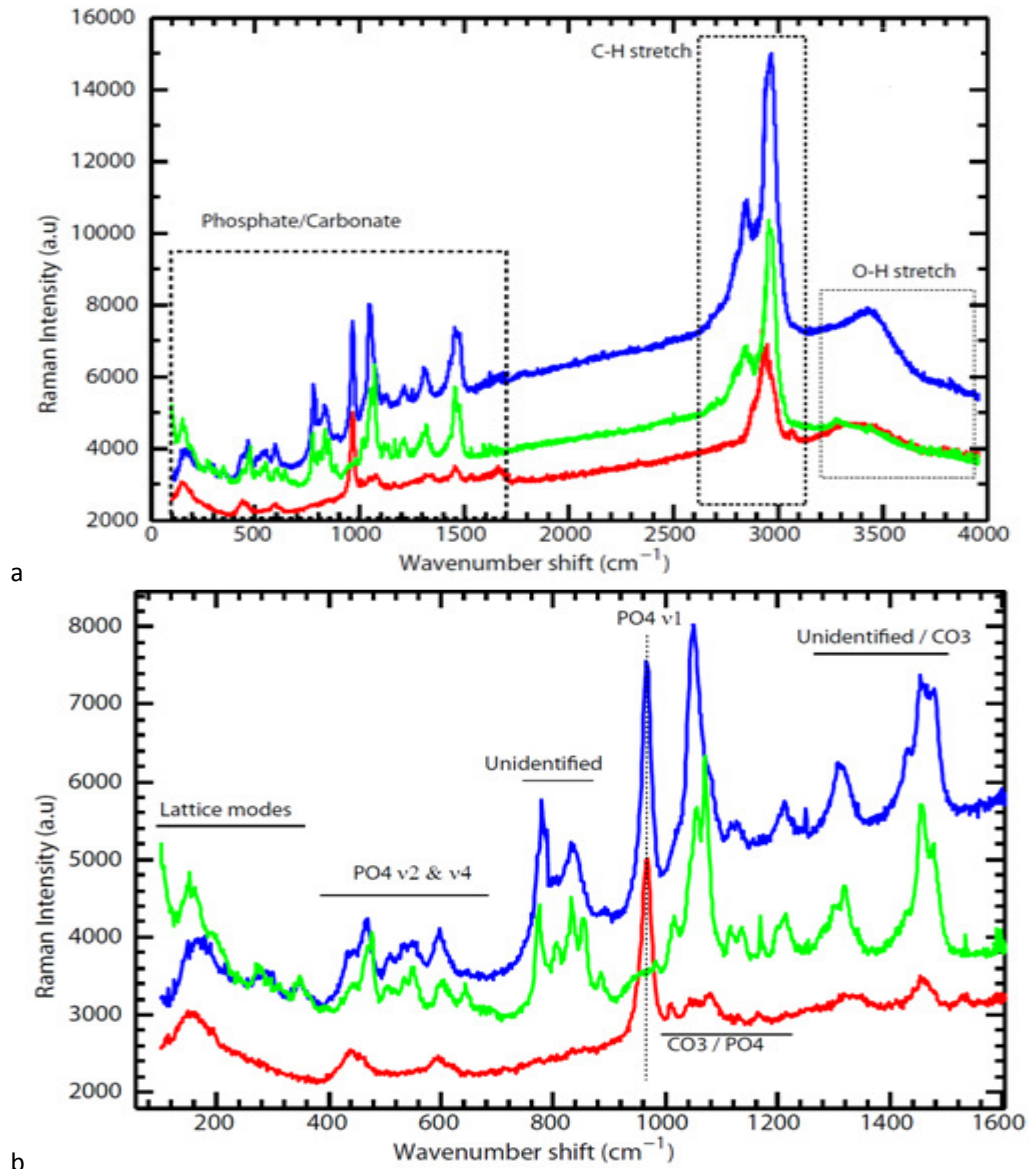
Figure 15: Raman spectroscopy results on titania surfaces after 4 weeks immersion in SBFs. a) focused on wavelength 0-4000 cm^{-1} , b) results within the wavelength 0-1600 cm^{-1}. Blue line is sample from SBF immersion, red line from SBF/Albumin and green line from SBF/Alendronate.

5. Conclusion

The results demonstrated that the mesoporosity on the titania surfaces initiated an enhanced calcium phosphate formation. More calcium phosphate was formed on the hexagonal than on the cubic mesoporous titania, however, both porous materials induced significantly higher formation compared to the non-porous titania. The observation was observed in the presence of simulated body fluid (SBF), SBF with Albumin and SBF with Alendronate.

The presence of Albumin in SBF decreased the ion adsorption and apatite formation and also decreased the size of the formed apatite crystals. The presence of porosity on the surfaces provided more opportunities for ion adsorption and apatite formation on the titania implant surfaces compared to on the non-porous surface.

The presence of Alendronate in the SBF decreased the ion adsorption, particularly on non-porous titania surface and hindered apatite formation.

6. Future work

It would be great to do some investigations on controlling the periodicity of the hexagonal and cubic pores on the surface.

Also, do some investigating on the effect of lower Alendronate concentration in SBF.

7. Acknowledgments

8. References

1.	Brunette, D.M., et al., *Titanium in medicine*. Vol. 35. 2001: Springer Berlin;.
2.	Grosso, D., et al., *A First Insight in the Mechanisms Involved in the Self-Assembly of 2D-Hexagonal Templated SiO 2 and TiO 2 Mesostructured Films During Dip-Coating.* Journal of sol-gel science and technology, 2003. **26**(1): p. 561-565.
3.	Dey, T., et al., *Anodic mesoporous TiO2 layer on Ti for enhanced formation of biomimetic hydroxyapatite.* Acta Biomaterialia, 2010.
4.	Wisbey, A., et al., *Effect of surface treatment on the dissolution of titanium-based implant materials.* Biomaterials, 1991. **12**(5): p. 470-473.
5.	Zhu, X., et al., *Characterization of nano hydroxyapatite/collagen surfaces and cellular behaviors.* Journal of Biomedical Materials Research Part A, 2006. **79**(1): p. 114-127.
6.	Alberius, P.C.A., et al., *General predictive syntheses of cubic, hexagonal, and lamellar silica and titania mesostructured thin films.* Chemistry of Materials, 2002. **14**(8): p. 3284-3294.
7.	Kokubo, T. and H. Takadama, *How useful is SBF in predicting in vivo bone bioactivity?* Biomaterials, 2006. **27**(15): p. 2907-2915.
8.	Bohner, M. and J. Lemaitre, *Can bioactivity be tested in vitro with SBF solution?* Biomaterials, 2009. **30**(12): p. 2175-2179.
9.	Oyane, A., et al., *Preparation and assessment of revised simulated body fluids.* Journal of Biomedical Materials Research Part A, 2003. **65A**(2): p. 188-195.
10.	Stenport, V., et al., *Precipitation of calcium phosphate in the presence of Albumin on titanium implants with four different possibly bioactive surface preparations. An in vitro study.* Journal of Materials Science: Materials in Medicine, 2008. **19**(12): p. 3497-3505.
11.	Liu, Y., et al., *Biomimetic coprecipitation of calcium phosphate and bovine serum Albumin on titanium alloy.* Journal of biomedical materials research, 2001. **57**(3): p. 327-335.
12.	Combes, C. and C. Rey, *Adsorption of proteins and calcium phosphate materials bioactivity.* Biomaterials, 2002. **23**(13): p. 2817-2823.
13.	Nancollas, G., et al., *Novel insights into actions of bisphosphonates on bone: differences in interactions with hydroxyapatite.* Bone, 2006. **38**(5): p. 617-627.
14.	Russell, R.G.G., et al., *The influence of pyrophosphate, condensed phosphates, phosphonates and other phosphate compounds on the dissolution of hydroxyapatitein vitro and on bone resorption induced by parathyroid hormone in tissue culture and in thyroparathyroidectomised rats.* Calcified tissue international, 1970. **6**(1): p. 183-196.
15.	McLeod, K., et al., *Adsorption of bisphosphonate onto hydroxyapatite using a novel co precipitation technique for bone growth enhancement.* Journal of Biomedical Materials Research Part A, 2006. **79**(2): p. 271-281.
16.	Boanini, E., et al., *Composite nanocrystals provide new insight on alendronate interaction with hydroxyapatite structure.* Advanced Materials, 2007. **19**(18): p. 2499-2502.
17.	.
18.	Iafisco, M., et al., *Adsorption and conformational change of myoglobin on biomimetic hydroxyapatite nanocrystals functionalized with alendronate.* Langmuir, 2008. **24**(9): p. 4924-4930.
19.	Linderbäck, P., et al., *Sol–gel derived titania coating with immobilized bisphosphonate enhances screw fixation in rat tibia.* Journal of Biomedical Materials Research Part A, 2010. **94**(2): p. 389-395.
20.	Jönsson, B., et al., *Surfactants and polymers in aqueous solution*. 1998: John Wiley & Sons New York.
21.	Shafrin, E.G. and W.A. Zisman, *Critical surface tension for spreading on a liquid substrate.* The Journal of Physical Chemistry, 1967. **71**(5): p. 1309-1316.

22.   Brunauer, S., P.H. Emmett, and E. Teller, *Adsorption of gases in multimolecular layers.* Journal of the American Chemical Society, 1938. **60**(2): p. 309-319.

23.   Barrett, E.P., L.G. Joyner, and P.P. Halenda, *The determination of pore volume and area distributions in porous substances. I. Computations from nitrogen isotherms.* Journal of the American Chemical Society, 1951. **73**(1): p. 373-380.

24.   Yang, Z., et al., *Mechanism and kinetics of apatite formation on nanocrystalline TiO2 coatings: A quartz crystal microbalance study.* Acta Biomaterialia, 2008. **4**(3): p. 560-568.

25.   Eliaz, N., et al., *Electrochemical processes of nucleation and growth of calcium phosphate on titanium supported by real time quartz crystal microbalance measurements and X ray photoelectron spectroscopy analysis.* Journal of Biomedical Materials Research Part A, 2009. **89**(1): p. 270-280.

26.   Coquil, T., et al., *Thermal conductivity of cubic and hexagonal mesoporous silica thin films.* Journal of Applied Physics, 2009. **106**(3): p. 034910-034910-11.

27.   Bottier, C., et al., *Galactosyl headgroup interactions control the molecular packing of wheat lipids in Lahgmuir films and in hydrated liquid-crystalline mesophases.* Biochimica Et Biophysica Acta-Biomembranes, 2007. **1768**(6): p. 1526-1540.

28.   Uchida, H., et al., *Highly-ordered mesoporous titania thin films prepared via surfactant assembly on conductive indium-tin-oxide/glass substrate and its optical properties.* Thin Solid Films, 2010. **518**(12): p. 3169-3176.

29.   Davey, R., *The effect of impurity adsorption on the kinetics of crystal growth from solution.* Journal of Crystal Growth, 1976. **34**(1): p. 109-119.

30.   Daculsi, G., et al., *Formation of carbonate-apatite crystals after implantation of calcium phosphate ceramics.* Calcified tissue international, 1990. **46**(1): p. 20-27.

31.   Paiva, A., et al., *Evaluation of the influence of Albumin on the mineralization of a glass by Atomic Force Microscopy.* Journal of Materials Science: Materials in Medicine, 2007. **18**(4): p. 599-604.

32.   Rapacz-Kmita, A., et al., *FTIR and XRD investigations on the thermal stability of hydroxyapatite during hot pressing and pressureless sintering processes.* Journal of Molecular Structure, 2005. **744**: p. 653-656.

33.   Melde, B.J. and A. Stein, *Periodic macroporous hydroxyapatite-containing calcium phosphates.* Chem. Mater, 2002. **14**(8): p. 3326-3331.

34.   Rey, C., et al., *The carbonate environment in bone mineral: a resolution-enhanced Fourier transform infrared spectroscopy study.* Calcified tissue international, 1989. **45**(3): p. 157-164.

35.   Cheng, Z.H., et al., *FTIR Study on incorporation of CO2 into calcium hydroxyapatite.* Journal of the Chemical Society-Faraday Transactions, 1998. **94**(10): p. 1501-1505.

36.   Slósarczyk, A., Z. Paszkiewicz, and C. Paluszkiewicz, *FTIR and XRD evaluation of carbonated hydroxyapatite powders synthesized by wet methods.* Journal of Molecular Structure, 2005. **744**: p. 657-661.

37.   Chang, M.C. and J. Tanaka, *FT-IR study for hydroxyapatite/collagen nanocomposite cross-linked by glutaraldehyde.* Biomaterials, 2002. **23**(24): p. 4811-4818.

38.   Militello, V., et al., *Aggregation kinetics of bovine serum Albumin studied by FTIR spectroscopy and light scattering.* Biophysical chemistry, 2004. **107**(2): p. 175-187.

39.   Sønju Clasen, A. and I. Ruyter, *Quantitative determination of type A and type B carbonate in human deciduous and permanent enamel by means of Fourier transform infrared spectrometry.* Advances in Dental Research, 1997. **11**(4): p. 523.

40.   Antonakos, A., E. Liarokapis, and T. Leventouri, *Micro-Raman and FTIR studies of synthetic and natural apatites.* Biomaterials, 2007. **28**(19): p. 3043-3054.